# UC Davis
## UC Davis Previously Published Works

**Title**

Naproxen chemoprevention induces proliferation of cytotoxic lymphocytes in Lynch Syndrome colorectal mucosa.

**Permalink**

https://escholarship.org/uc/item/9hg9k0zk

**Authors**

Bowen, Charles M
Deng, Nan
Reyes-Uribe, Laura
et al.

**Publication Date**

2023

**DOI**

10.3389/fimmu.2023.1162669

**Copyright Information**

Peer reviewed

Check for updates

# Naproxen chemoprevention induces proliferation of cytotoxic lymphocytes in Lynch Syndrome colorectal mucosa

Charles M. Bowen[1], Nan Deng[1], Laura Reyes-Uribe[1],
Edwin Roger Parra[2], Pedro Rocha[2], Luisa M. Solis[2],
Ignacio I. Wistuba[2], Valerie O. Sepeda[1], Lana Vornik[1],
Marjorie Perloff[3], Eva Szabo[3], Asad Umar[3], Krishna M. Sinha[1],
Powel H. Brown[1] and Eduardo Vilar[1,4]*

[1]Department of Clinical Cancer Prevention, The University of Texas MD Anderson Cancer Center,
Houston, TX, United States, [2]Translational Molecular Pathology, The University of Texas MD Anderson
Cancer Center, Houston, TX, United States, [3]Division of Cancer Prevention, National Cancer Institute,
Bethesda, MD, United States, [4]Clinical Cancer Genetics Program, The University of Texas MD
Anderson Cancer Center, Houston, TX, United States

**Background:** Recent clinical trial data from Lynch Syndrome (LS) carriers demonstrated that naproxen administered for 6-months is a safe primary chemoprevention that promotes activation of different resident immune cell types without increasing lymphoid cellularity. While intriguing, the precise immune cell types enriched by naproxen remained unanswered. Here, we have utilized cutting-edge technology to elucidate the immune cell types activated by naproxen in mucosal tissue of LS patients.

**Methods:** Normal colorectal mucosa samples (pre- and post-treatment) from a subset of patients enrolled in the randomized and placebo-controlled 'Naproxen Study' were obtained and subjected to a tissue microarray for image mass cytometry (IMC) analysis. IMC data was processed using tissue segmentation and functional markers to ascertain cell type abundance. Computational outputs were then used to quantitatively compare immune cell abundance in pre- and post-naproxen specimens.

**Results:** Using data-driven exploration, unsupervised clustering identified four populations of immune cell types with statistically significant changes between treatment and control groups. These four populations collectively describe a unique cell population of proliferating lymphocytes within mucosal samples from LS patients exposed to naproxen.

**Conclusions:** Our findings show that daily exposure of naproxen promotes T-cell proliferation in the colonic mucosa, which paves way for developing combination of immunoprevention strategies including naproxen for LS patients.

KEYWORDS

Lynch Syndrome (hereditary nonpolyposis colorectal cancer), immunoprevention, image mass cytometry, bioinformactics, cancer prevention

# Introduction

Lynch Syndrome (LS, MIM 120435), the most common hereditary colorectal cancer (CRC) syndrome, affects approximately one million people in the United States (1). The underlying molecular pathophysiology of LS has been leveraged as a model syndrome for understanding carcinogenesis in the setting of DNA mismatch repair (MMR) deficiency (2, 3). Despite surveillance guideline recommendations of annual colonoscopy for LS carriers, rapid interval tumors, inadequate compliance remain an unmet clinical challenge and compromising the survival of the LS patient population. Therefore, the aforementioned challenges pose the need for developing durable interventions such as immune- and chemo-preventive modalities.

Previous studies, such as the Colorectal Adenoma/Carcinoma Prevention Program-2 (CAPP-2) study found that the chronic use of aspirin, a non-steroidal anti-inflammatory drug (NSAID), had favorable efficacy as a chemoprevention for all LS-related tumors (4, 5). These studies established the framework for launching the 'Naproxen Study', a phase IB, placebo-controlled, randomized clinical trial (NCT02052908) in LS carriers (6). Results from this trial demonstrated that both high and low dose naproxen administered for 6-months is a safe primary chemoprevention that promotes activation of different resident immune cell types without increasing general lymphoid cellularity *via* reduction of proinflammatory prostaglandin levels. In addition, naproxen effectively modulated tumor growth while prolonging survival in a pre-clinical trial using a tissue-specific mouse model of LS (6).

At the time of publication of the original trial data, immune cell enrichment analysis based on mRNAseq data from normal colorectal mucosa using *in silico* cell deconvolution was not able to elucidate the resident immune cell types activated by naproxen, which remained an unanswered, yet highly intriguing question for improving future development of preventive measures in LS. Precisely discerning the types of activated immune cells upon naproxen administration was limited in the previous study, which did not incorporate tissue acquisition procedures for high-resolution single-cell omics, due to lack of technical approaches at the time of study implementation. However, in-house advancements of single-cell omics has afforded the ability to generate an integrative spatial profiles of immune cells within mucosal samples collected from a subset of available participant's samples using image mass cytometry (IMC) and recently developed bioinformatic techniques (7–9). From these computational benchmarks, we have discovered that daily chemoprevention with naproxen at low (220 mg) and high (440 mg) dosing activates proliferation of resident cytotoxic lymphocytes in colonic mucosa, which opens new opportunities for refining immune-prevention strategies of patients with LS.

# Materials and methods

## Study design and participants

Patient samples used in this study come from participants enrolled to the original 'Naproxen Study'. Participants provided written informed consent to participate in the study, and ethical approval was obtained from the Institutional Review Boards (IRB) of all participating centers (IRB MDACC 2013-0698 and PA12-0327). Details on the trial design and participant demographics have been already reported (6). Here, we present the sub-analysis of data only from participants enrolled to the trial at The University of Texas MD Anderson Cancer Center, one of the four trial sites.

## Tissue micro array

A total of 36 Formalin-fixed Paraffin-embedded (FFPE) colon biopsies from Lynch Syndrome participants (18 pre-treatment and 18 post-treatment tissue samples) were collected. Three unstained slides (4 μm thickness) sections were obtained from each sample to perform hematoxylin and eosin (H&E) and immunohistochemistry (IHC) staining. A pathologist (L.S.) evaluated H&E slides to determine the quality of the sample, selection of areas for tissue microarray (TMA) construction, and histomorphometry analysis. Two biopsy blocks were excluded due to artifacts and insufficient tissue for analysis. One single TMA block was created using up to two tissue cores (1 mm diameter) from each colon biopsy specimen for further Image Mass Cytometry (IMC) staining. Normal and neoplastic control tissues (appendix, lymph node, tonsil, spleen, placenta, breast carcinoma, and ovary carcinoma) for IMC staining were included in the TMA of colon biopsies block to evaluate the staining quality from each immune marker.

## Image mass cytometry staining

An Immuno-Oncology (IO)-IMC panel with 36 validated markers was designed to include lymphoid (CD45RO, CD3, CD4, CD8, CD19, Granzyme B, CD94, OX40), myeloid (CD11b, CD14, CD68, MPO, CD11c, HLA-DR, CD163, CD33), immune-modulatory (CCR6, PD-L1, CD73, FOXP3, TIM3, LAG3, VISTA, B7-H3, ICOS), epithelial (pan cytokeratin, panCK), proliferative (Ki67), and leukocyte/constitutive (CD45, β2-microglobulin, GAPDH, NaKATPase) markers. The IO-IMC panel was optimized by single plex-IHC assays of BSA-free monoclonal antibodies, followed by single plex indirect immunofluorescence (IF) assays of each metal-isotope-tagged antibody (Maxpar Labeling Kits; Fluidigm), and a final multiplex staining step containing the whole cocktail with 36 metal-isotope-tagged antibodies. A control TMA (4 μm diameter) including normal and neoplastic tissues (tonsil, appendix, placenta, prostate, breast carcinoma, ovarian carcinoma, and endometrioid carcinoma) was used for each staining assay, and to select the optimal concentration per antibody showing a constant cellular subtype expression, and a stable pattern of staining in the same control tissue cores observed by single- and multiplex staining. Fifty consecutive 4 μm thickness unstained slides were obtained from the TMA block of colon biopsy specimens. To select the unstained slides for IMC staining, three slides at different levels (1, 25, and 50) were stained with H&E. The level 25 showed the highest number of cases (46) with at least one core evaluable, therefore a standardized IMC manual staining protocol was performed in three adjacent levels (22, 23, and 24). The staining protocol included one single antigen retrieval step (Tris buffer, pH 9.0, two-cycles of 10 min at 99°C), an overnight IMC panel cocktail

incubation step at 4°C followed by Iridium and Ruthenium counterstaining. One field of view (FOV) per core (800 μm x 800 μm) was ablated and imaged by Hyperion Imaging System (Fluidigm) and MCD Viewer Software (v1.0.560.2, Fluidigm) for further digital image analysis.

## Image mass cytometry data processing

A TIFF-format image file for each mass channel was generated from the MCD file and then segmented into single cells using the ImcSegmentaionPipeline (https://github.com/BodenmillerGroup/ImcSegmentationPipeline) (10). Briefly, we generated a probability map by classifying pixels using Ilastik v.1.1.929 based on a combination of antibody staining to identify membranes, nuclei (single cells), and filter the background (Table 1). Then, these probability maps were segmented into single-cell object masks using CellProfiler (Version 3.1.9). The epithelium compartments were identified and segmented by combining NaKATPase-176Yb and panCK-174Yb signals into CellProfiler. Finally, the mean density of each marker was summarized at the single-cell level for future analysis.

## Data normalization and processing

Regarding gating analysis, no data transformation or normalization was applied. Additionally, all data were analyzed as a single batch, and thus, batch correction was not required. The Centered log-ratio (CLR) method implemented in the R package Seurat (Version 4.1.1) (8) was used for UMAP visualization. To visualize the data, we performed the Barnes-Hut implementation of t-distributed neighborhood embedding (tSNE) based on the markers and plotted this embedding in 2-dimensional space (perplexity, 50; number of iterations, 1,000).

## Clustering

Single cells from every field of view (FOV) were combined and clustered by the PhenoGraph algorithm (9) using R package Rphenograph (Version 0.99.1.9003) by their mean marker correlations. The UMAP algorithm was used for visualization of the data. Then, cell populations of interest were manually named based on the expression of markers, and their relative abundance

TABLE 1 Immune mass cytometry metal-labeled antibodies.

| N | Marker | Metal | Description | Clone | Vendor | Titration (1:X) | Cat# |
|---|--------|-------|-------------|-------|--------|-----------------|------|
| 1 | CD45RO | 139La | Memory T-cells | T200/797 | Abcam | 500 | ab212786 |
| 2 | CCR6 | 141Pr | Treg | EPR22259 | Abcam | 1000 | ab243852 |
| 3 | CD137 | 142Nd | Check point | BLR051F | Bethyl | 25 | A700-051. |
| 4 | ICOS | 143Nd | Check point | D1K2T | CST | 50 | 89601BF |
| 5 | PD-L1 | 144Nd(2X) | Check point | E1L3N | CST | 50 | 13684BF |
| 6 | CD68 | 145Nd | Macrophage | EPR20545 | Abcam | 1000 | ab227458 |
| 7 | MPO | 146Nd | Neutrophil | EPR20257 | Abcam | 2500 | ab221847 |
| 8 | PD-1 | 147Sm | Check point | EPR4877 | Abcam | 25 | ab186928 |
| 9 | CD11c | 148Nd | Dendritic cell | EP1347Y | Abcam | 2000 | ab216655 |
| 10 | CD73 | 149Sm | Check point | BLR054F | Bethyl | 500 | A700-54. |
| 11 | HLA-DR | 150Nd | Antigen Presentation | EPR3692 | Abcam | 350 | ab215985 |
| 12 | CD163 | 151Eu | Macrophage | BLR087G | Bethyl | 400 | A700-087. |
| 13 | Granzyme B | 152Sm | T-cell Activation | D6E9W | CST | 1000 | 46890BF |
| 14 | CD11b | 153Eu | Macrophage | EPR1344 | Abcam | 500 | ab216445 |
| 15 | CD14 | 154Sm | Macrophage | EPR3653 | Abcam | 1500 | ab214438 |
| 16 | FOXP3 | 155Gd | Treg | BLR034F | Bethyl | 25 | A700-034. |
| 17 | TIM3 | 156Gd | Checkpoint | D5D5R | CST | 200 | 45208BF |
| 18 | CD66b | 158Gd | Activated neutrophil | EPR7701 | Abcam | 100 | ab249555 |
| 19 | LAG3 | 159Tb | T-cell Activation | D2G4O | CST | 200 | 15372BF |
| 20 | CD39 | 160Gd | Treg | EPR20461 | Abcam | 250 | ab232573 |
| 21 | IDO-1 | 161Dy | Treg | D5J4E | CST | 25 | 86630BF |
| 22 | Ki-67 | 162Dy | Proliferation | D2H10 | CST | 200 | 9027BF |

*(Continued)*

TABLE 1 Continued

| N | Marker | Metal | Description | Clone | Vendor | Titration (1:X) | Cat# |
|---|--------|-------|-------------|-------|--------|-----------------|------|
| 23 | VISTA | 163Dy | Checkpoint | D1L2G | CST | 50 | 64953BF |
| 24 | β2-microglobulin | 164Dy | Other, MHC-I | D8P1H | CST | 200 | 12851BF |
| 25 | CD19 | 165Ho | B-cells | D4V4B | CST | 1500 | 90176BF |
| 26 | CD8a | 166Er | CD8 cells | D8A8Y | CST | 100 | 85336BF |
| 27 | CD33 | 167Er | Myeloid lineage | SP266 | Abcam | 600 | ab238784 |
| 28 | B7-H3 | 168Er | Check point | D9M2L | CST | 25 | 14058BF |
| 29 | CD45 | 169Tm | Lymphocytes | EP322Y | Abcam | 800 | ab214437 |
| 30 | CD94 | 170Er | NK cell/cytotoxic lymphocytes | EPR21003 | Abcam | 50 | ab238166 |
| 31 | OX40 | 171Yb | T-cell Activation | E9U7O | CST | 25 | 61637BF |
| 32 | CD3e | 172Yb | Lymphocytes | D7A6E | CST | 100 | 85061BF |
| 33 | CD4 | 173Yb | T-helper Lymphocyte | EPR6855 | Abcam | 1000 | ab181724 |
| 34 | Cytokeratin | 174Yb | Epithelial | AE1/AE3 | Abcam | 25 | ab80826 |
| 35 | GAPDH | 175Lu | Other, control | 14C10 | CST | 5000 | 2118BF |
| 36 | NaKATPase | 176Yb | Other, control | EP1845Y | Abcam | 200 | ab167390 |

Thirty-six validated markers designed to include lymphoid, myeloid, immune-modulatory, epithelial, proliferative, and leukocyte/constitutive.
'#' is a short-hand abbreviation for number.

was calculated as the number of a given cell type of interest divided by the total number of cells in each compartment.
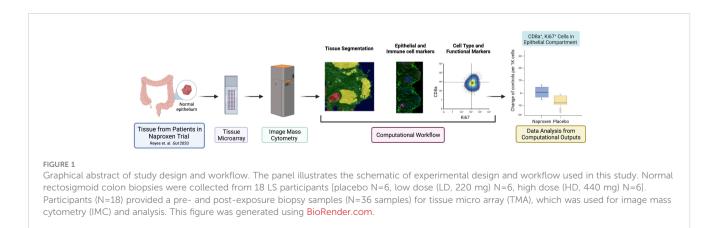
## Statistical analysis

Changes in the cluster proportions relative to the total number of cells in the epithelial and non-epithelial compartment were calculated. Wilcoxon tests were performed using the R (Version 4.0.5) base package. Bonferroni multiple testing adjustment was applied as indicated in each analysis.

## Results

The experimental design and computational workflow are graphically described in Figure 1 and detailed in the Materials and Methods section. Tissue biopsies from 18 patients (pre- and post-treatment; N=36 samples) enrolled in the 'Naproxen Study' were obtained for IMC analysis (Supplementary Tables 1, 2). Tissue segmentation helped segregate the epithelial compartment from the stroma utilizing a multitude of markers for lymphoid (i.e. CD19, CD3) and epithelium (i.e. pan cytokeratin, panCK), which shows clear delineation between the two cellular compartments within the biopsy samples (Figure 2A and Table 1). Then, tissue sections were stained with 36 different metal-isotope-tagged antibodies (Table 1) to identify the localization of epithelial and immune cell types (Figure 2B) within the epithelial compartment previously identified from the segmentation analysis.

Using data-driven exploration, unsupervised clustering by the Phenograph algorithm generated clusters of 165 cell populations (9). From this output, we found four distinct immune cell populations of interest with statistically significantly changes between the treatment and control groups (Figure 3A;



FIGURE 1
Graphical abstract of study design and workflow. The panel illustrates the schematic of experimental design and workflow used in this study. Normal rectosigmoid colon biopsies were collected from 18 LS participants [placebo N=6, low dose (LD, 220 mg) N=6, high dose (HD, 440 mg) N=6]. Participants (N=18) provided a pre- and post-exposure biopsy samples (N=36 samples) for tissue micro array (TMA), which was used for image mass cytometry (IMC) and analysis. This figure was generated using BioRender.com.

Supplementary Figure 1A). These cells are CD8a^{+} T cells in the epithelium, and immune cells that are outside of epithelium are HLA-DR^{+}/CD8a^{+} T cells, CD11c- macrophages, and CD11c^{+}/IDO-1^{+}/PD-L1^{+}. The absolute relative change between naproxen versus placebo for each group (Figure 3A, left to right) was 10.74 ± 4.73, 12.10 ± 4.77, 14.62 ± 4.91, and 11.17 ± 4.06, respectively, suggesting sustained cellularity of mucosal resident immune cell types by chronic use of naproxen in LS patients. To elucidate if this sustained observation was dose-dependent, we then analyzed the data by separating the naproxen groups (low-dose, 220 mg versus high-dose, 440 mg) and determined no significant difference in relative cellular abundance when comparing low-dose to high-dose groups (Supplemental Figures 1B, C). Furthermore, the function of each cell population was elucidated by quantifying the expression of gene markers related to lymphocyte and monocyte cellular markers (Figure 3B) that identified six different groups representing lymphocytes, T cell activation, T cell memory, monocyte, immune checkpoint and others. In accordance with our manual gating analysis, the levels of epithelial Ki67^{+}/CD8a^{+}/CD3e^{+} T cell population remained the same in the treatment group, but not in the placebo group, which showed an absolute reduction in levels over the course of the trial (P-value=0.032, Figures 3A, B; Supplementary Figure 1A). The relatively higher levels of CD45RO/CCR6 in the naproxen treatment than control group are indicative of an enrichment of T cell memory phenotype (11). Interestingly, activated memory T-cells correlated with high levels of OX40 (12), CD137 (13) and Granzyme B (14) expression (Figure 3B; Supplementary Figures 2, 3), thereby suggesting activation of T-cell function in anti-tumor immunity. High resolution IMC histology thus corroborated computational-based deconvolution findings, showing proliferating lymphocytes (CD8^{+}/Ki67^{+}) within mucosal samples from LS patients exposed to naproxen as visualized by the co-localization of Ki67 and CD8 staining (Figure 3C).

## Discussion

We have identified that proliferating (Ki67^{+}), activated (OX40^{+}/GZMB^{+}/CD137^{+}), memory (CD45RO/CCR6^{+}) CD8a^{+} T-cells become activated upon naproxen treatment (12, 15). The importance of CD8^{+} T-cells in CRC biology has been well addressed in previously reported studies (16, 17) with a positive association between CD8a^{+} T-cell infiltration and favorable clinical outcomes (18). The stability in the numbers of activated CD8a^{+} T cells observed in our sub-cohort could be attributed to the reduction of prostaglandin E2 (PGE2) levels after using naproxen, thus confirming that reduction in PGE2 levels by naproxen has general anti-inflammatory effects, while promoting T cell retention in the colorectal mucosa (6). In addition to local effects of naproxen in the colonic mucosa, previous studies have shown elevated PGE2 levels in patient serum suppresses naïve memory and effector T cells with selective suppression of effector functions (19). In the original 'Naproxen Trial', global reduction in PGE2 levels correlated with activation of cytokine-related pathways and overall immune activation especially in B- and T-cell lineages (6). While the data reported in this manuscript explored the intrinsic local changes in immune activation within the colonic mucosa, it is possible that the effects of naproxen to peripheral immune cells contributed to the activation of immune cells within the mucosa of LS patients. Thus, the sustained immune cellularity after naproxen treatment is likely maintained by reduction of PGE2 levels at the peripheral and tissue-specific levels.
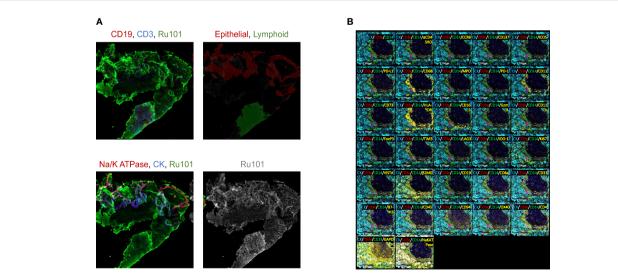


FIGURE 2
Immune mass cytometry isolated discrete immune cell populations following tissue segmentation. **(A)** Fluorescent image of tissue section stained for epithelial and immune cell markers. Upper left: red for CD19, blue for CD3, green for Ru101; Upper right: red for epithelial, green for lymphoid tissue; Bottom left: red for Na/K ATPase, blue for CK, green for Ru101; Bottom right shows Ru101; **(B)** Tissue section slides stained with multiplex metal-labeled antibody markers. Panel shows the representative image of IMC from an individual sample. Segmentation was performed to demarcate epithelium (cytokeratin, CK) from stroma. Metal-labeled antibody markers are listed in Table 1.
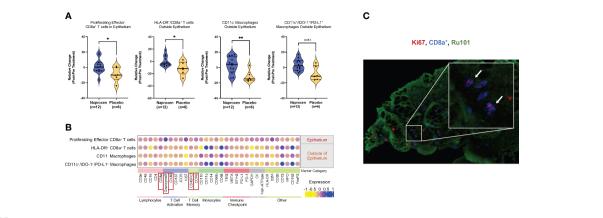
**FIGURE 3**

Chemopreventive naproxen increases activation of cytotoxic T-lymphocytes in the mucosa. **(A)** Data-driven analysis of the cell population within the mucosa. Change in cell ratio in those immune cell types for the naproxen and placebo groups that showed statistically significant changes. Solid line denotes median and dashed line denotes quartiles. *P*-values from paired Wilcoxon test from left to right: P=0.032, P=0.048, P=0.0047, P=0.052 (*, *P*-value<0.05; **, *P*-value<0.01); **(B)** Dot-plot graph shows the expression level of stained makers for the four cell types with statistically significant changes between naproxen and placebo groups. The color gradient represents the mean expression level of the corresponding marker in the population. Markers are grouped into categories based on cell type; Red boxes indicate expression markers of highlighted in the text; **(C)** High-resolution IMC image of Ki67+ (red), CD8a+ (blue), and Ru101 (green) in a LS mucosal sample. The white arrows indicate double-positive CD8+/Ki67 + cells in the colonic mucosa.

While an overall sustained immune response was observed for most trial participants, some of them demonstrated insufficient maintenance of immune cellularity despite receiving naproxen treatment (Supplemental Figure 1C). While the molecular mechanisms at play are beyond the scope of this manuscript, nuanced differences in the tissue microenvironment has been hypothesized to be the cause of immune evasion in some LS carriers (20), and therefore naproxen could help overcome it by exerting stimulation of the resident immune cells in the colorectal mucosa. Furthermore, the heterogeneity in lifelong neoantigen priming (21), known as 'self-education' of the immune system, is variable from person to person, and may partially help explain the lack of response (i.e. observed decrease in immune cellularity) to naproxen in some of the LS participants. Similarly, through self-priming mechanisms, it is also possible that LS patients experience T-cell anergy, which occurs along a continuum depending on relative neoantigen abundance. Nonetheless, these hypotheses warrant further investigation.

Although the original 'Naproxen Trial' demonstrated a dose-dependent effect between low-dose and high-dose naproxen-mediated immune activation, this study showed no dose-dependent effect, which is most likely explained by the small size or random biological variation between patients. It is also possible that naproxen-mediated immune activation encompasses a broad therapeutic window, which warrants further studies to assess dose effect on T lymphocyte activation.

This study utilized image mass cytometry (IMC) to quantify relative abundance of immune cells in the colonic mucosa. This powerful technique enabled high-resolution multiplexing of metal-tagged antibodies to determine naproxen sustained T-lymphocyte cellularity within the mucosal compartment of LS patients. Unlike more traditional methods such as immunofluorescence, IMC affords quantification of 40 markers within 135 detection channels. Moreover, the use of metal-tagged antibodies reduces spectral overlap and background signaling, which are often confounding disadvantages of immunofluorescence. Another advantage to IMC over more conventional methods is the customizability of metal conjugation reagents and spatial scanning of multiple regions of interest on the same slide (22, 23). While IMC has powerful capabilities and advantages, the equipment cost, panel optimization, and complex computation skills are major barriers of use.

While this study has further identified the overall impactful role of naproxen within the normal colonic mucosa, mechanistic studies, which remain lacking, are necessary to better understanding the molecular underpinnings at play that govern immune activation and enrichment especially given the heterogeneity between different LS patients. The exploration of those studies is warranted for further studies, though it is an important and undetermined questions in the field.

In summary, this work deepens our understanding of the cellular composition within the mucosal epithelium of LS carriers upon administration of naproxen for chemoprevention. Despite a more stringent schedule of annual or bi-annual colonoscopy screenings, patients with LS still develop CRC for various reasons such as rapid interval tumors (6). The need for robust, durable preventive strategies remains a dire unmet need for the clinical management of hereditary CRC syndromes. Moving forward, this study helps pave the way for adaptive immunoprevention strategies for LS carriers combining neoantigen vaccines with naproxen as immune stimulant (24, 25).

# Data availability statement

The datasets presented in this study can be found in online repositories. The names of the repository/repositories and accession number(s) can be found below: https://www.ncbi.nlm.nih.gov/geo/, GSE144381. https://zenodo.org/record/7655637#.ZEf9PXbMI2x.

# Ethics statement

# Author contributions

# Funding

# Acknowledgments

# Conflict of interest

EV had a consulting or advisory role with Janssen Research and Development, Recursion Pharma, and Guardant Health. He has received research support from Janssen Research and Development.

The remaining authors declare that the research was conducted in the absence of any commercial or financial relationships that could be constructed as a potential conflict of interest.

# Publisher's note

All claims expressed in this article are solely those of the authors and do not necessarily represent those of their affiliated organizations, or those of the publisher, the editors and the reviewers. Any product that may be evaluated in this article, or claim that may be made by its manufacturer, is not guaranteed or endorsed by the publisher.

# Supplementary material

The Supplementary Material for this article can be found online at: https://www.frontiersin.org/articles/10.3389/fimmu.2023.1162669/full#supplementary-material

# References

1. Spira A, Yurgelun MB, Alexandrov L, Rao A, Bejar R, Polyak K, et al. Precancer atlas to drive precision prevention trials. *Cancer Res* (2017) 77:1510–41. doi: 10.1158/0008-5472.CAN-16-2346

2. Bommi PV, Bowen CM, Reyes-Uribe L, Wu W, Katayama H, Rocha P, et al. The transcriptomic landscape of mismatch repair-deficient intestinal stem cells. *Cancer Res* (2021) 81:2760–73. doi: 10.1158/0008-5472.CAN-20-2896

3. Fearon ER. Molecular genetics of colorectal cancer. *Annu Rev Pathol: Mech Dis* (2011) 6:479–507. doi: 10.1146/annurev-pathol-011110-130235

4. Burn J, Bishop DT, Mecklin J-P, Macrae F, Möslein G, Olschwang S, et al. Effect of aspirin or resistant starch on colorectal neoplasia in the lynch syndrome. *N Engl J Med* (2008) 359:2567–78. doi: 10.1056/NEJMoa0801297

5. Burn J, Gerdes A-M, Macrae F, Mecklin J-P, Moeslein G, Olschwang S, et al. Long-term effect of aspirin on cancer risk in carriers of hereditary colorectal cancer: an analysis from the CAPP2 randomised controlled trial. *Lancet* (2011) 378:2081–7. doi: 10.1016/S0140-6736(11)61049-0

6. Reyes-Uribe L, Wu W, Gelincik O, Bommi PV, Francisco-Cruz A, Solis LM, et al. Naproxen chemoprevention promotes immune activation in lynch syndrome colorectal mucosa. *Gut* (2021) 70:555–66. doi: 10.1136/gutjnl-2020-320946

7. Giesen C, Wang HAO, Schapiro D, Zivanovic N, Jacobs A, Hattendorf B, et al. Highly multiplexed imaging of tumor tissues with subcellular resolution by mass cytometry. *Nat Methods* (2014) 11:417–22. doi: 10.1038/nmeth.2869

8. Hao Y, Hao S, Andersen-Nissen E, Mauck WM, Zheng S, Butler A, et al. Integrated analysis of multimodal single-cell data. *Cell* (2021) 184:3573–3587.e29. doi: 10.1016/j.cell.2021.04.048

9. Levine JH, Simonds EF, Bendall SC, Davis KL, Amir ED, Tadmor MD, et al. Data-driven phenotypic dissection of AML reveals progenitor-like cells that correlate with prognosis. *Cell* (2015) 162:184–97. doi: 10.1016/j.cell.2015.05.047

10. Zanotelli VRT, Bodenmiller B. ImcSegmentationPipeline: a pixelclassification based multiplexed image segmentation pipeline. (2017). doi: 10.5281/zenodo.3841961

11. Kondo T, Takata H, Takiguchi M. Functional expression of chemokine receptor CCR6 on human effector memory CD8+ T cells. *Eur J Immunol* (2007) 37:54–65. doi: 10.1002/eji.200636251

12. Paterson DJ, Jefferies WA, Green JR, Brandon MR, Corthesy P, Puklavec M, et al. Antigens of activated rat T lymphocytes including a molecule of 50,000 Mr detected only on CD4 positive T blasts. *Mol Immunol* (1987) 24:1281–90. doi: 10.1016/0161-5890(87)90122-2

13. Eiva MA, Omran DK, Chacon JA, Powell DJ. Systematic analysis of CD39, CD103, CD137, and PD-1 as biomarkers for naturally occurring tumor antigen-specific TILs. *Eur J Immunol* (2022) 52:96–108. doi: 10.1002/eji.202149329

14. Oudejans JJ, Harijadi H, Kummer JA, Tan IB, Bloemena E, Middeldorp JM, et al. High numbers of granzyme B/CD8-positive tumour-infiltrating lymphocytes in nasopharyngeal carcinoma biopsies predict rapid fatal outcome in patients treated with curative intent. *J Pathol* (2002) 198:468–75. doi: 10.1002/path.1236

15. Ye Q, Song D-G, Poussin M, Yamamoto T, Best A, Li C, et al. CD137 accurately identifies and enriches for naturally occurring tumor-reactive T cells in tumor. *Clin Cancer Res* (2014) 20:44–55. doi: 10.1158/1078-0432.CCR-13-0945

16. Budhu S, Loike JD, Pandolfi A, Han S, Catalano G, Constantinescu A, et al. CD8 + T cell concentration determines their efficiency in killing cognate antigen–expressing syngeneic mammalian cells *in vitro* and in mouse tissues. *J Exp Med* (2010) 207:223–35. doi: 10.1084/jem.20091279

17. Kloor M, von Knebel Doeberitz M. The immune biology of microsatellite-unstable cancer. *Trends Cancer* (2016) 2:121–33. doi: 10.1016/j.trecan.2016.02.004

18. Ohtani H. Focus on TILs: prognostic significance of tumor infiltrating lymphocytes in human colorectal cancer. *Cancer Immun* (2007) 7:4.

19. Kalinski P. Regulation of immune responses by prostaglandin E2. *J Immunol* (2012) 188:21–8. doi: 10.4049/jimmunol.1101029

20. Hernandez-Sanchez A, Grossman M, Yeung K, Sei SS, Lipkin S, Kloor M. Vaccines for immunoprevention of DNA mismatch repair deficient cancers. *J Immunother Cancer* (2022) 10:e004416. doi: 10.1136/jitc-2021-004416

21. Bohaumilitzky L, von Knebel Doeberitz M, Kloor M, Ahadova A. Implications of hereditary origin on the immune phenotype of mismatch repair-deficient cancers: systematic literature review. *J Clin Med* (2020) 9:E1741. doi: 10.3390/jcm9061741

22. Veenstra J, Dimitrion P, Yao Y, Zhou L, Ozog D, Mi Q-S. Research techniques made simple: use of imaging mass cytometry for dermatological research and clinical applications. *J Invest Dermatol* (2021) 141:705–712.e1. doi: 10.1016/j.jid.2020.12.008

23. Schlecht A, Boneva S, Salie H, Killmer S, Wolf J, Hajdu RI, et al. Imaging mass cytometry for high-dimensional tissue profiling in the eye. *BMC Ophthalmol* (2021) 21:338. doi: 10.1186/s12886-021-02099-8

24. Kloor M, Reuschenbach M, Pauligk C, Karbach J, Rafiyan M-R, Al-Batran S-E, et al. A frameshift peptide neoantigen-based vaccine for mismatch repair-deficient cancers: a phase I/IIa clinical trial. *Clin Cancer Res* (2020) 26:4503–10. doi: 10.1158/1078-0432.CCR-19-3517

25. Enokida T, Moreira A, Bhardwaj N. Vaccines for immunoprevention of cancer. *J Clin Invest* (2021) 131:e146956. doi: 10.1172/JCI146956